DEPTH-DEPENDENT SOIL FLUIDIZATION UNDER CYCLIC LOADING- AN EXPERIMENTAL INVESTIGATION

Warantorn Korkitsuntornsan

Research Associate,

Transport Research Centre, University of Technology Sydney, Ultimo, NSW 2007, Australia

Buddhima Indraratna[1]

Distinguished Professor of Civil Engineering, and Director,

Transport Research Centre, University of Technology Sydney, Ultimo, NSW 2007, Australia

Cholachat Rujikiatkamjorn

Professor,

School of Civil and Environmental Engineering, University of Technology Sydney, Ultimo, NSW 2007, Australia

Thanh T. Nguyen

Research Fellow,

Transport Research Centre, University of Technology Sydney, Ultimo, NSW 2007, Australia

Words: 1716

Figures: 5

Submitted to: Canadian Geotechnical Journal (Technical Note)

[1]Corresponding author: Buddhima Indraratna (e-mail: buddhima.indraratna@uts.edu.au)

Abstract

Past studies have shown that shallow subgrade soil can transform to a slurry (i.e., fluidization) under unfavourable cyclic loading. However, the depth-dependent behaviour of soil parameters during this process has not been properly understood. The current study utilised a large-scale cylindrical test rig, where instrumentation was installed to observe the soil behaviour along the depth of the test specimens under cyclic loading, to examine and quantify the onset of soil fluidization. The results show that excess pore water pressure (EPWP) tends to rise more at the upper layers causing zero-effective stress, while void ratio expands rapidly within the deteriorated soil fabric making the water content approach the liquid limit of soil when internal moisture migration occurs from the bottom to the top of specimen. The larger the cyclic load, the deeper the fluidized zone and the faster the fluidization. The study also suggests that the zero-effective stress condition alone cannot interpret the inception of soil fluidization, hence the change in void ratio and the liquidity index during the application of cyclic loading should also be considered in tandem.

Keywords: Consolidation, Clays, Pore Pressures; Repeated Loading, Fabric/structure of soils

1. Introduction

Recent experimental investigations show that subjected to unfavourable cyclic loading induced by heavy haul trains, upper soil layer near the surface tends to degrade considerably with increasing excess pore water pressure (EPWP) to initiate fluidization (Duong et al. 2014; Huang et al. 2019; Indraratna et al. 2020a; Wheeler et al. 2017). While this phenomenon has been reported worldwide (Nguyen et al. 2019), the actual mechanism that causes soil to rapidly fluidize has still been debatable due to the lack of rigorous experimental assessments and field monitoring. Rising EPWP degrading the soil fabric accompanied with dilation and substantial decrease in soil stiffness is probably the major factor causing subgrade fluidization beneath rail tracks. Experimental simulations (Indraratna et al. 2020b) demonstrated that the upward migration of moisture during cyclic loading, causing the moisture content of the upper soil layers approaches its liquid limit (LL), contributed to this phenomenon. However, none of these studies could capture the continuous (time-dependent) increase in void ratio (i.e., dilation) occurring in tandem with the rising EPWP. Furthermore, the development of soil fluidization across the soil depth (i.e., localized behaviour) has not been quantified in past studies.

In view of the above, this study describes innovatively how the localized change in void ratio and the rising EPWP may occur simultaneously when the soil fluidizes under cyclic excitation. A cyclic model is established to describe the inception of fluidization, incorporating the measured data over the depth of the test specimen. The laboratory measurements are used to interpret the triggering condition of fluidization based on the variations of void ratio, excess pore pressure distribution and the effective stress.

2. Experimental investigation

Estuarine clayey soil samples were collected at a depth of 1 to 2m from the coastal town of Ballina (NSW). This soil was classified as a high plasticity clay (CH), and had a natural water content of 59% and a bulk density of 1,660 kg/m^3. Its liquid and plastic limits (LL and PL) were 82 and 35%. Clay, silt and sand contents of the soil were 18, 77 and 4%, respectively.

A stainless steel cell was used to contain the soil specimen, where instrumentation was placed in various locations (Fig. 1). Two transducers (T1 and T2) were installed to measure the total pressure at different depths (50 mm and 200 mm). Four miniature pore pressure transducers (i.e., P1, P2, P3 and P4), which ensured minimum disturbance to the soil, were installed along the depth to measure EPWP. To observe the response of different soil layers, an observation window (stiff transparent perspex) was fabricated on one side of the cell. A high-resolution camera was set up to capture visually the soil response over time.

The test procedure consisted of two stages as described below.

(i) Pre-consolidation stage: The collected soil was mixed with water to a moisture content of 98%. Subsequently, the soil slurry was transferred to the consolidation cell, and 4 layers of sand were added as shown in Fig. 1. Grease was applied to the cell interior to minimize boundary friction. A vertical pressure of 15 kPa to simulate the field overburden pressure was then applied to the soil, while the drainage was allowed at the top and bottom of the specimen until the volume change upon consolidation became insignificant. The saturation of the soil specimen was verified by amplitude domain reflectometry probes.

(ii) Cyclic loading stage: A cyclic (uniform sinusoidal) load was then applied to the top of the specimen in undrained condition. Two loading amplitudes, i.e., 50 and 60 kPa typically representing the propagated vertical stress on the soil subgrade in the field were considered, while a frequency f of 2.0 Hz was adopted to represent the attenuated frequency on the subgrade caused by an average train speed of 80 km/h (Nguyen and Indraratna 2022). Each

test was terminated when the number of cycles (N) reached 40,000 cycles.

3. Experimental findings and discussion

Depth-dependent response of soft soil subjected to cyclic loading

The variations of EPWP at different depths are shown in Fig. 2. The greater the soil depth, the lower the build-up of EPWP. For example, for q = 50 kPa, the EPWP at a depth of 50 mm rapidly increases and exceeds 11 kPa after about 2,500 cycles that causes the zero-effective stress condition. EPWP then reaches the peak of 22.5 kPa at around 10,000 cycles before stabilising towards the end (N = 40,000 cycles). EPWPs at greater depths (i.e., 200 and 250 mm) also show the samse response, but at a lower magnitude. Furthermore, the results show that EPWP reaches the peak faster at higher loading. For example, for q = 60 kPa, about 6,000 cycles is required to reach the peak EPWP. The corresponding effective stress (p') that drops to zero at 2,500 and 1,500 cycles for q = 50 and 60 kPa, respectively. Corresponding to the generation of EPWP, there is a sharp increase in axial strain (ε_a) within the first 2,500 cycles before attaining a gradual stabilization. The larger the applied load, the greater the axial strain for the same number of cycles. For example, after N = 2500, ε_a = 0.48% and 0.62% for q = 50 and 60 kPa, respectively. Although the soil sample had lost its strength (i.e., the effective stress becoming zero), the axial strain tends to stabilize after the peak due to the use of rigid cell (lateral confinement) and undrained condition.

Fig. 3 shows a typical example of how fluidization progressively develops around the surface zone of the test specimen under q = 50 kPa. There is significant disturbance of the soil close to the surface (i.e., an expanded dark region with a dispersed sand layer) accompanied by an internal rearrangement of the soil along the height of the specimen. At 2,500 cycles, the grey and dark region representing the fluidized soil begins to appear in the shallower soil (Layer 1). Meanwhile, EPWP at this depth rises rapidly to exceed the critical level of 11 kPa (Fig. 2), further disturbing the soil fabric. The fluidized region continues to spread towards the deeper part of the soil specimen as *N* continues to rise to 20,000 cycles, now resulting in complete fluidization of Layer 1 and partially of Layer 2. On the other hand, there is no sign of soil fluidization in deeper Layers 3 and 4 despite *N* rising to 40,000 cycles; instead, these lower layers become more compacted (decreased thickness) as captured through image processing. This emphatically indicates the localized distinct response whereby the soil fluidization initiates at the top soil layers, while cyclic densification occurs at the lower depths of the specimen.

Figure 4 shows a non-uniform distribution of void ratio along the specimen height, while the total void ratio of the specimen slightly decreases. In this analysis, the void ratio was computed using the initial void ratio (after consolidation) and change in thickness of soil layers captured by processing images (observed through the cell window). Specifically, for *q* = 50 kPa, the void ratio of Layer 1 increases from its initial value of 1.92 to 2.0 after 2,500 cycles, and this corresponds to the slurry formation in this zone (Fig. 3). In contrast, the void ratio of the lower Layers 3 and 4 gradually decreases, thus signifying cyclic densification. Interestingly, the void ratio of Layer 2 decreases (compression) during the first 10,000 cycles before rising to around 2.0 at the end of loading, which reflects the dilation of the fluidized soil over time towards the deeper region. Similar depth-dependent behaviour was captured when *q* increased to 60 kPa, however, the fluidized region was found to propagate deeper towards the Layer 3 at the end of testing. The measurement after testing showed that the topmost layer had the largest water content (82.5% and 87.9% for 50 and 60 kPa loading) that exceeded the LL of the soil (82%), whereas the water content at the bottom layer decreased to 66.8 %, compared to its initial value of 73.8%.

Condition of soil fluidization

The above results show that when the soil fluidizes, there are two vital changes occurring in the soil parameters, namely, (*i*) the effective stress (i.e., EPWP) and (*ii*) the void ratio. The soil liquidity index (LI), which represents the threshold of fluidization in relation to the current water content and LL, was computed using the void ratio (Fig. 4), and the results were then combined with the effective stress, as shown in Fig. 5. The LI at Layer 1 rapidly increases to unity representing the slurry-like state, whereas the LI at the bottom steadily decreases when undergoing cyclic densification. Meanwhile, p' in both top (Layer 1) and bottom (Layer 4) soil regions decreases due to rising EPWP. Despite p' reaching the zero-effective stress condition, the lowermost soil with a stable LI does not show any sign of fluidization (Fig. 3). This implies that the conventional use of mean effective stress alone cannot clearly distinguish the difference between the stable and fluidized soil regions under cyclic loading. In this regard, the use of LI or void ratio in tandem is surely more appropriate to better capture fabric degradation under cyclic loading, and the associated inception of soil fluidization.

4. Conclusions

The following salient conclusions could be drawn throughout this study.

1. When the soft soil was subjected to cyclic loading, the EPWP increased more towards the surface region of the soil leading to dilation, while the bottom part of the soil underwent cyclic densification as moisture (pore fluid) migrated upwards. At the critical level of EPWP (i.e., 11 kPa) representing the condition of zero-effective stress, the upper soil region showed significant fabric disturbance. In tandem, void ratio increased rapidly from 1.92 to 2.13, causing the water content to rise towards the LL of 82%, thus fluidization.
2. A greater magnitude of cyclic load implied that the potential depth of fluidization could increase at a lower number of loading cycles.
3. The study also verified that the zero-effective stress condition should be considered in

tandem with the liquidity index approaching unity when assessing the onset of soil fluidization.

Data Availability

Data available will be provided upon request.

Acknowledgements

This research was supported by the Australian Research Council (**LP160101254**), Transport Research Centre (TRC-UTS) and industry partners including SMEC, Coffey, ACRI and Sydney Trains.

Figures

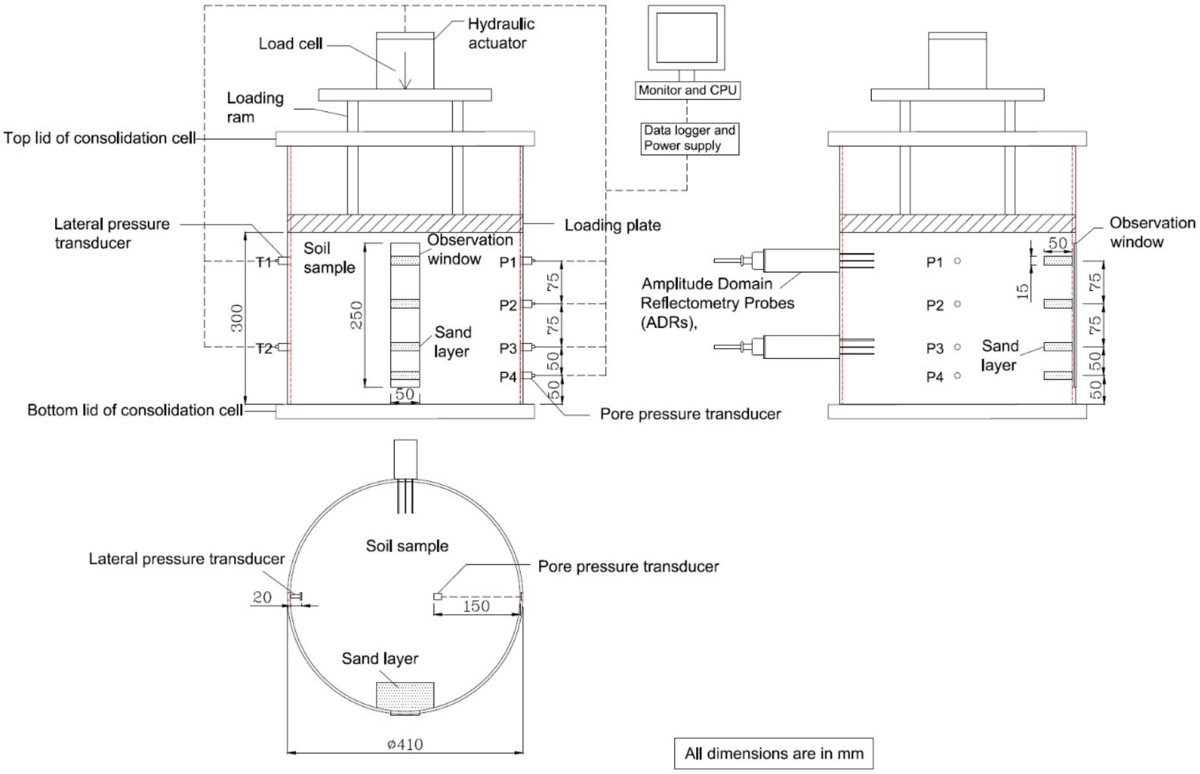

Fig. 1 Detailed schematic diagram of the test rig incorporating observations and instrumentations over the depth

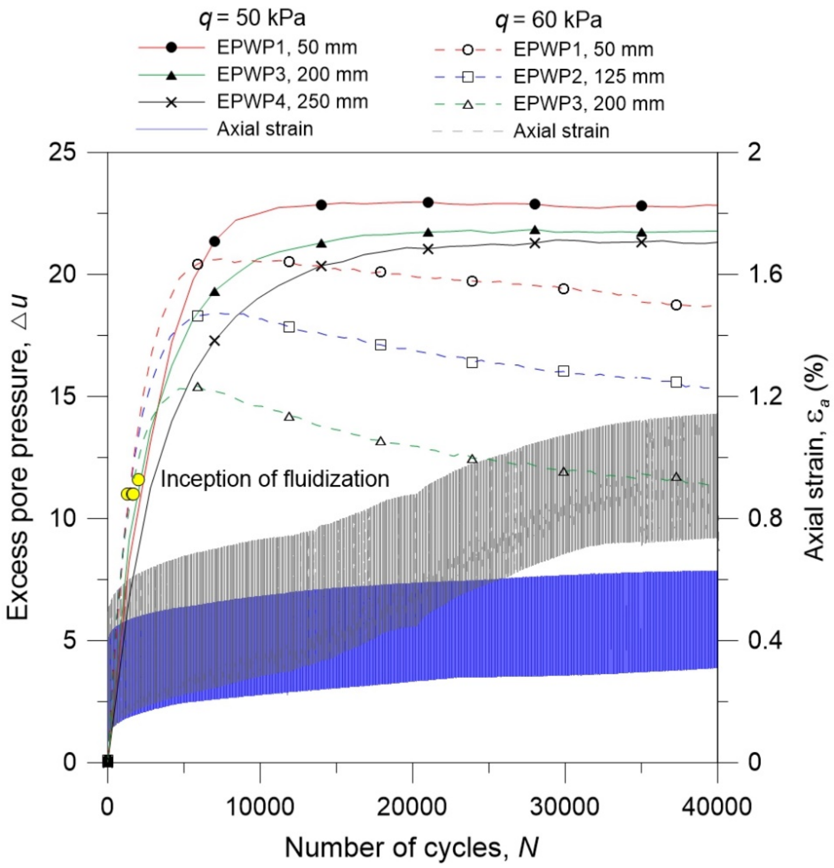

Fig. 2 Excess pore water pressure and axial strain with depth

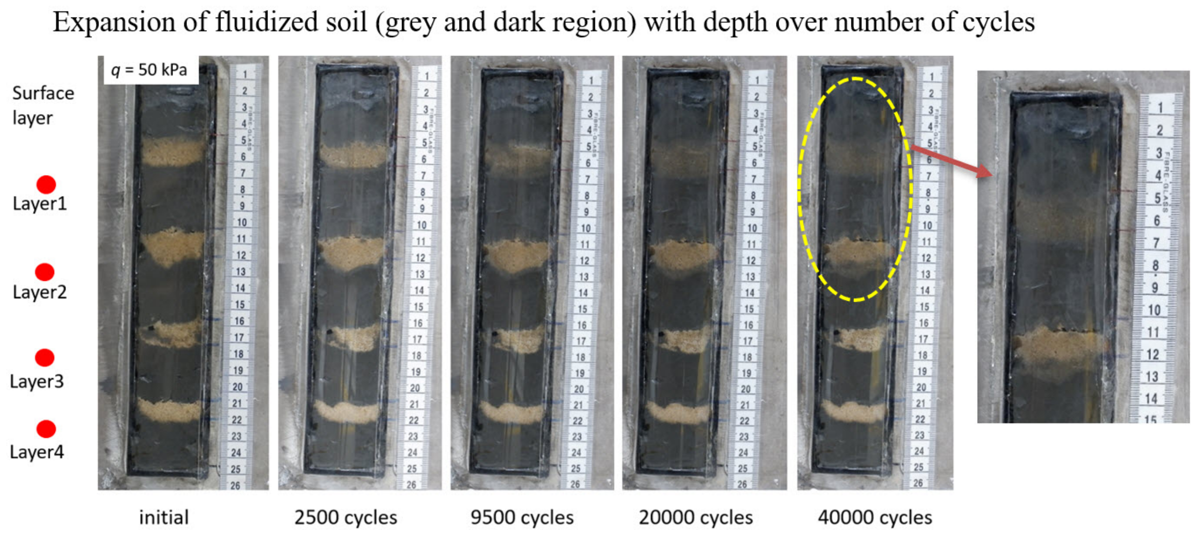

Fig. 3 Example of window observations captured over time with loading cycles (q = 50 kPa)

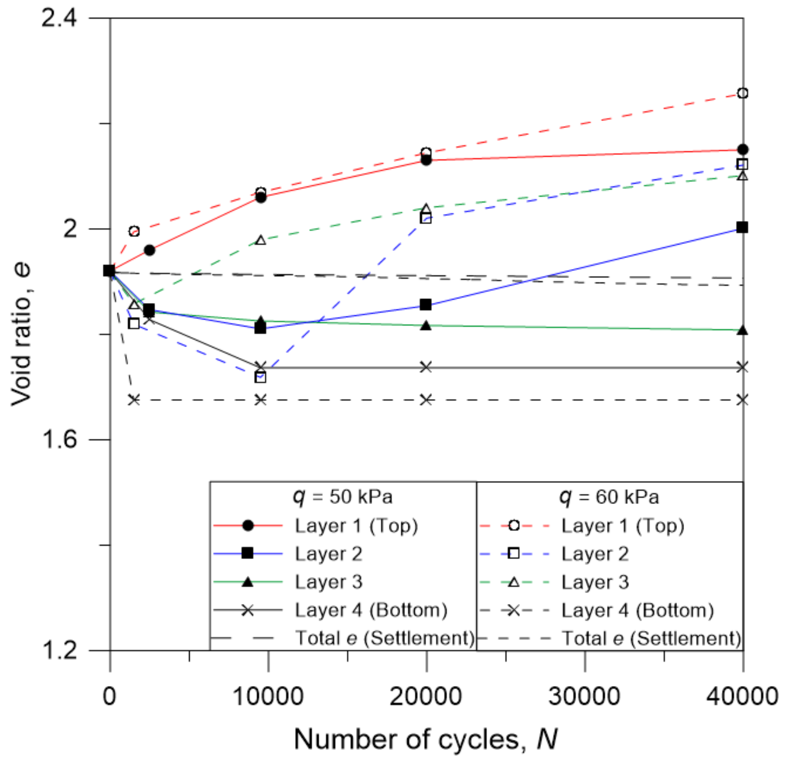

Fig. 4 Variation of void ratio (top, middle, bottom layers) for applied load of q = 50 and q = 60 kPa

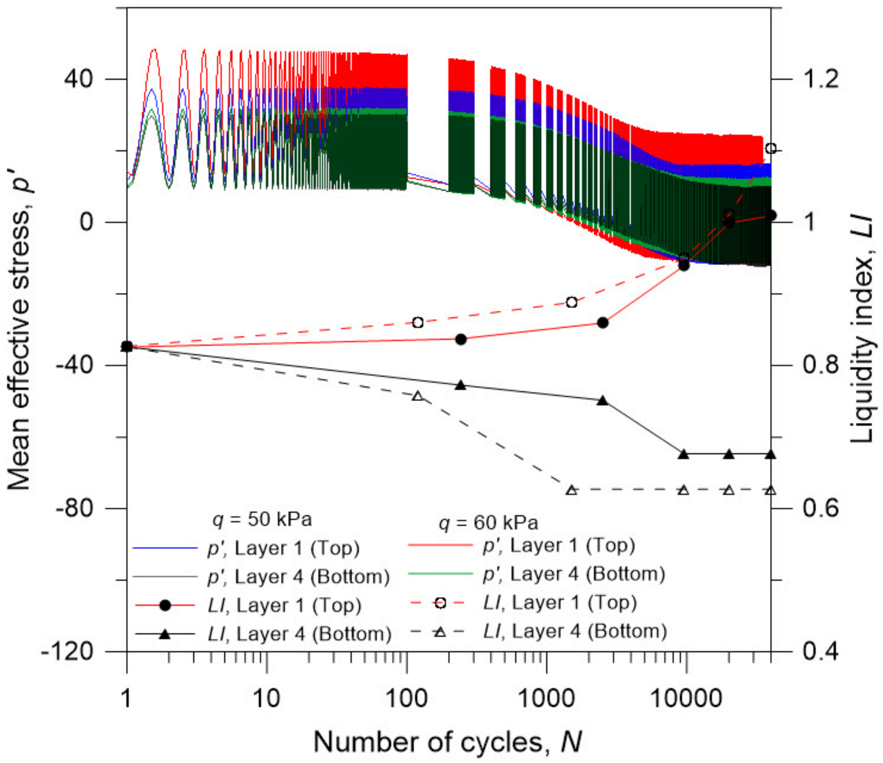

Fig. 5 Liquidity index and effective stress over increasing N

REFERENCES

Duong, T.V., Cui, Y.-J., Tang, A.M., Dupla, J.-C., Canou, J., Calon, N., and Robinet, A. 2014. Investigating the mud pumping and interlayer creation phenomena in railway sub-structure. Engineering geology, **171**: 45-58.doi:https://doi.org/10.1016/j.enggeo.2013.12.016.

Huang, J., Su, Q., Wang, W., Phong, P.D., and Liu, K. 2019. Field investigation and full-scale model testing of mud pumping and its effect on the dynamic properties of the slab track–subgrade interface. Proceedings of the Institution of Mechanical Engineers, Part F: Journal of Rail and Rapid Transit, 233(8): 802-816. doi:10.1177/0954409718810262.

Indraratna, B., Korkitsuntornsan, W., and Nguyen, T.T. 2020a. Influence of Kaolin content on the cyclic loading response of railway subgrade. Transportation Geotechnics, 22: 100319. doi:https://doi.org/10.1016/j.trgeo.2020.100319.

Indraratna, B., Singh, M., Nguyen, T.T., Leroueil, S., Abeywickrama, A., Kelly, R., and Neville, T. 2020b. Laboratory study on subgrade fluidization under undrained cyclic triaxial loading. Canadian Geotechnical Journal, 57(11): 1767-1779. doi:10.1139/cgj-2019-0350.

Nguyen, T., Indraratna, B., Kelly, R., Phan, N.M., and Haryono, F. 2019. Mud pumping under railtracks: mechanisms, assessments and solutions. Australian Geomechanics Journal, **54**: 59-80.

Nguyen, T.T., and Indraratna, B. 2022. Rail track degradation under mud pumping evaluated through site and laboratory investigations. International Journal of Rail Transportation: 1-28. doi:https://doi.org/10.1080/23248378.2021.1878947.

Wheeler, L.N., Take, W.A., and Hoult, N.A. 2017. Performance assessment of peat rail subgrade before and after mass stabilization. Canadian Geotechnical Journal, 54(5): 674-689. doi:10.1139/cgj-2016-0256.